npj | parkinson's disease

Article

Published in partnership with the Parkinson's Foundation

https://doi.org/10.1038/s41531-025-01002-2

Mapping striatal functional gradients and associated gene expression in Parkinson's disease with continuous cognitive impairment

Check for updates

Xiaolu Li[1], Shuting Bu[1], Huize Pang[1], Hongmei Yu[2], Mengwan Zhao[1], Juzhou Wang[1], Yu Liu[1] & Guoguang Fan[1] ✉

Cognitive impairment in Parkinson's disease is closely tied to striatal dysfunction, yet the neurobiological interface between macroscale connectivity and molecular signatures remains unexplored. This study characterizes striatal gradient organization and its genetic underpinnings across PD cognitive trajectories. We analyzed functional connectivity gradients in 126 PD patients (spanning the cognitive spectrum from normal cognition to dementia) and 40 healthy controls, correlating spatial patterns with neurotransmitter architecture and transcriptomic profiles. Three distinct striatal gradients emerged: Gradient 1 remains stable throughout disease progression and partially aligns with canonical striatal subdivisions. Gradient 2 represents a spatial continuum closely linked to dopaminergic innervation and becomes most pronounced in the dementia stage. Gradient 3 corresponds to cortico-striatal connectivity patterns implicated in both early and advanced cognitive deficits. Spatial transcriptomic and neuroimaging correlation analyses identified significant associations between cortico-striatal gradient disruptions and specific gene expression patterns. These findings provide valuable insights into striatal macro- and microstructural changes in PD and their role in cognitive impairment.

Cognitive impairment is the most common non-motor symptom in Parkinson's disease (PD), significantly impacting functionality, quality of life, caregiver burden, and health-related costs[1]. Despite its prevalence, the causes of cognitive impairment in PD remain unclear, with considerable variability in symptoms, severity, progression, and underlying pathology[2]. This spectrum ranges from subtle changes to mild cognitive impairment (PD-MCI) and extends to more severe deficits observed in Parkinson's disease dementia (PDD)[3]. The heterogeneity of cognitive impairment in PD highlights the need to understand its mechanisms and identify biomarkers that can predict cognitive performance and its progression.

The striatum plays a crucial role in cognitive functions such as reward processing, executive function, decision making, and goal-directed behavior[4–6]. Numerous studies have highlighted that both microscopic and macroscopic changes in the striatum are linked to cognitive decline in PD. At the macroscopic level, abnormal neural communication within the striatum circuit is a major pathological feature of PD, resulting from its extensive structural and functional connectivity with both cortical and subcortical areas[7]. Prior studies have linked impairments in corticostriatal and striatal–thalamo–cortical loops to both motor and non-motor symptoms in PD, including depression[8], anxiety[9], cognitive impairment[10], apathy[11,12], tremor[13], rigidity[14], impulse control disorders[15], and behavioral disturbances[16]. Besides macroscopic changes, microscopic alterations in the striatum, such as protein deposits[17,18], synaptic reduction[19–21], and neurotransmitter dysfunction[22–25], also contribute to cognitive impairment. However, the relationship between microscopic and macroscopic changes in PD cognitive impairment is still poorly understood. Clarifying these associations is crucial for advancing our understanding of the pathophysiological mechanisms underlying this disorder.

Although structural and functional analyses have identified striatal changes in PD-related cognitive impairment, conventional approaches using hard parcellations assume constant activity across relatively large brain areas. These methods cannot account for overlapping representations within the striatum and fail to capture its cortical complexity. These issues are particularly significant in the striatum due to its gradual connectivity pattern suggested by tracing studies, and the convergence of projections from widespread cortical regions. To characterize the brain's gradual connectivity

[1]Department of Radiology, The First Hospital of China Medical University, Liaoning, China. [2]Department of Neurology, The First Hospital of China Medical University, Liaoning, China. ✉e-mail: fanguog@sina.com

patterns, which also called hierarchical organization, researchers have recently applied dimensionality reduction techniques to high-dimensional resting-state functional connectivity (rsFC) data from resting-state functional magnetic resonance imaging (rs-fMRI). This approach derives a simplified set of principal components that capture continuous transitions and broad spatial relationships of rsFC patterns across brain regions, referred to as functional connectivity gradients. Each gradient is a continuous representation of one facet of brain topographical organization and each brain location can be depicted by a value reflective of where it falls along this continuum[26]. Previous research has identified a hierarchical structure within the striatum, with significant spatial variation (i.e., gradients) in PD, primarily along the anterior-posterior axis[27–29]. Furthermore, Marianne Oldehinkel et al. reported that second-order mode functional connectivity in the striatum is associated with dopaminergic projections and can serve as a non-invasive biomarker for investigating dopaminergic dysfunction[30]. Additionally, striatal connectivity has been linked to the hierarchical organization of the cortex, displaying gradients of sensorimotor, associative, and limbic domains along the anterior-posterior (rostral-caudal) and ventromedial-dorsolateral axes[29,31,32].

The function of the striatum is closely related to its cellular and biochemical properties[29]. To investigate the molecular mechanisms underlying changes in striatum gradients, we used spatial transcriptomic association analysis and various enrichment analyses. Unlike genome-wide neuroimaging association studies that require large sample sizes, transcription-neuroimaging association studies can identify genes associated with neuroimaging changes in brain disorders using relatively small samples[33]. Using densely sampled gene expression data from six post-mortem brains available in the Allen Human Brain Atlas (AHBA; http://human.brain-map.org), several studies have identified genes linked to altered anatomical[34,35], functional disconnectivity[36], abnormal morphometric similarity differences[37] and interhemispheric connectivity loss[38] in PD. However, no transcription-neuroimaging association study has been conducted to identify genes associated with striatal gradient alterations in PD.

In this study, we used rs-fMRI data to construct functional connectivity gradients of the striatum in PD patients with a spectrum of cognitive impairment. We then mapped the striatum functional connectivity gradients across canonical functional networks to provide detailed topographic maps of the cortico-striatal circuitry. To explore the potential genes regulating striatum functional connectivity gradients, we referenced the AHBA and identified enrichment pathways through connectome and transcriptome association analyses. A schematic summary of the processing pipeline is shown in Fig. 1.

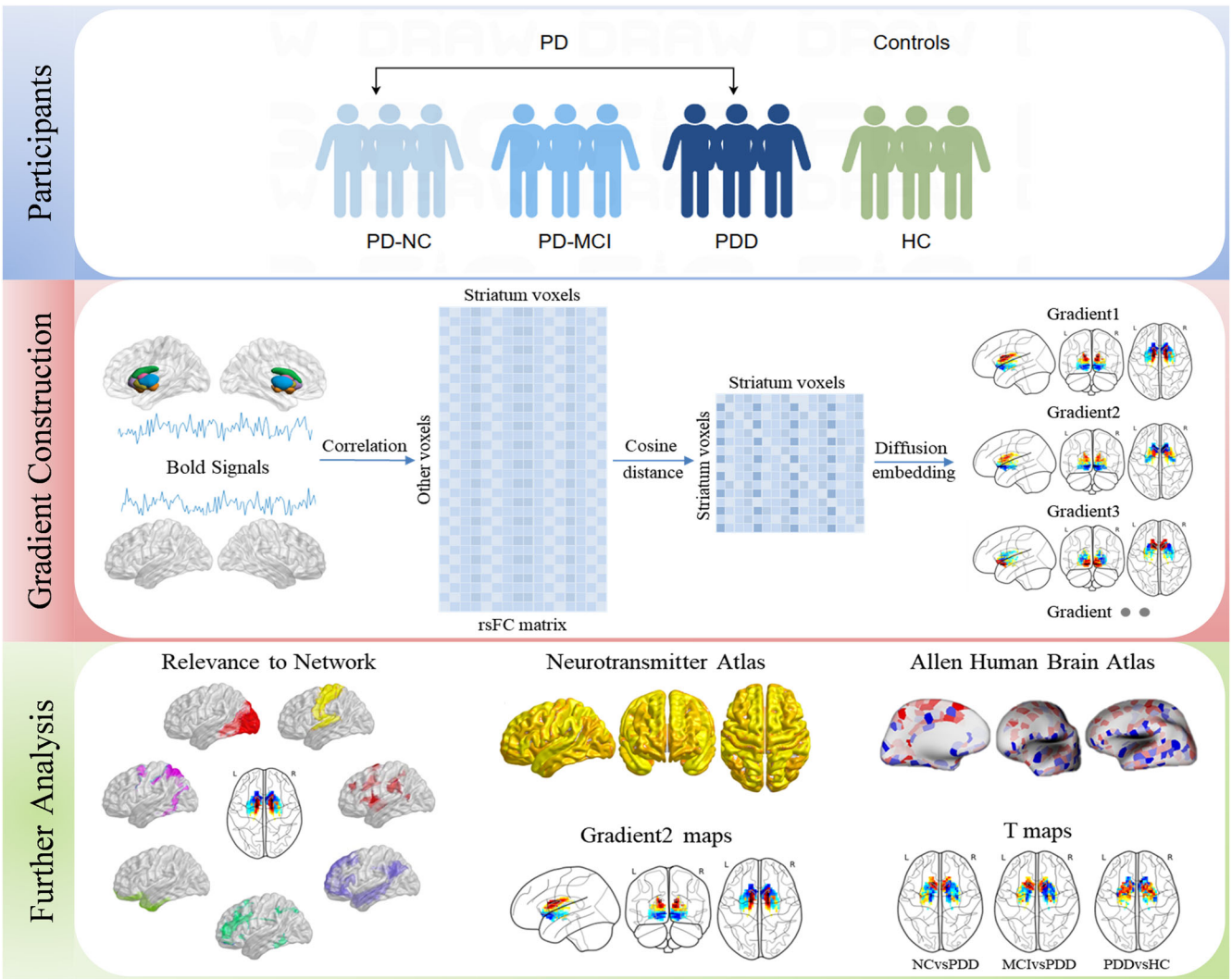

Fig. 1 | Research design and analytical procedure. Top panel: Participants. A total of 115 PD patients and 36 HC were included, categorized into PD-NC, PD-MCI, and PDD groups. Middle panel: Gradient construction. Functional connectivity gradients of the striatal cortex were computed using voxel-wise striatal cortex-to-cerebrum rsFC profiles and diffusion embedding. Bottom panel: Further analyzes. We investigated the associations of striatal functional connectivity gradients with canonical functional networks, the neurotransmitter atlas, and the Allen Human Brain Atlas. BOLD blood-oxygen-level-dependent, rsFC resting-state functional connectivity, HC healthy controls, NC normal cognitive, MCI mild cognitive impairment, PDD Parkinson's disease dementia.

Results

Demographic and clinical data

The demographic and clinical data of the participants were presented in Table 1. There were no significant differences among patient cohorts in terms of age, gender, years of education, H-Y stage, disease duration, MDS-UPDRS III scores, or LEDD ($P > 0.05$). However, years of education were lower in the PDD group compared to healthy controls ($P < 0.05$). Differences in MMSE, MoCA, and specific cognitive subdomain scores were reported in Table 1.

Connectome gradient maps

Consistent with prior research, our study focused on the top three connectome gradients[26]. Figures 2a–c illustrate the mean gradient maps for each group. Specifically, Gradient 1 demonstrates continuous spatial variation from the caudate to the putamen and nucleus accumbens, resembling the anatomical subdivisions of the striatum. Gradient 2, in contrast, spans from the dorsal putamen and dorsal caudate (shown in red) to the ventral putamen, ventral caudate, and nucleus accumbens (shown in blue). This pattern suggests that the dorsal putamen and caudate share similar connectivity with the rest of the brain, distinct from that of the ventral putamen and caudate. This striatal connectivity pattern is similar with the second-order mode, which has recently been associated with dopaminergic innervation of the striatum, as revealed by a high spatial correlation ($r = 0.884$) between the gradient and DAT-SPECT-derived dopamine transporter (DAT) availability (Supplementary Fig. S1, *the second-order connectivity mode*)[30]. Gradient 3 defines a continuous spatial pattern, spanning from ventromedial systems (shown in red) to dorsolateral systems (shown in blue), resembling the well-established cortico-striatal circuitry gradient (Supplementary Fig. S1, *the first-order connectivity mode*)[6]. Furthermore, we observed a strong similarity in the mean gradient maps across the four subgroups (all $r > 0.74$, all p corrected $< 1 \times 10^{-15}$). The spatial similarities between the mean gradient maps for each group are provided in the Supplementary Fig. S2.

Global gradient measurements

The variance explained by the top three gradients in each group is provided in Supplementary Note1. No statistically significant differences were observed in the range, variability, and explanatory rate from the three principal gradients among groups (Table 2). For Gradient 1, the results were as follows: range: $F = 0.227$, $P = 0.878$; variability: $F = 0.136$, $P = 0.938$; explanatory rate: $F = 0.896$, $P = 0.445$. For Gradient 2, the results were as follows: range: $F = 0.786$, $P = 0.504$; variability: $F = 0.995$, $P = 0.397$; explanatory rate: $F = 2.599$, $P = 0.055$. For Gradient 3, the results were as follows: range: $F = 0.697$, $P = 0.555$; variability: $F = 0.506$, $P = 0.679$; explanatory rate: $F = 0.167$, $P = 0.919$.

Relevance to functional networks

Given that Gradient 3 resembles the typical striatal-cortical gradient, which spans a continuous spatial pattern from ventromedial systems to dorsolateral systems, we focused primarily on its functional implications. Within Gradient 3, the yeo-seven-network parcellation is shown in Fig. 3A, the functional subdivision corresponding to the SMN was not found. Across the four groups, averaged gradients revealed a functional differentiation progressing from the dorsal attention network (DAN) and VN towards the ventral attention network (VAN) (Fig. 3B, C).

Voxel-level and network-level group-related difference in striatal gradient

Voxel-wise comparisons (FDR correction, $P < 0.05$) revealed significant findings among PD subgroups (Fig. 4, Table 3): There were no significant differences between any groups in Gradient 1. In Gradient 2, PDD patients exhibited higher gradient scores in the right nucleus accumbens (NAC.R) and lower gradient scores in the right dorsolateral putamen (dlPu.R) compared to PD-MCI patients. Notably, after controlling for covariates, Gradient 2 scores in the NAC.R were negatively correlated with overall MoCA scores ($r = -0.444$, $P < 0.001$), as well as with memory scores ($r = -0.248$, $P = 0.029$) in PD patients (Supplementary Fig. S3). In Gradient 3, PDD patients showed higher

Table 1 | Demographic and clinical characteristics

Variables	NC($n = 45$)	MCI($n = 50$)	PDD($n = 31$)	HC($n = 40$)	NCvsMCI	MCIvsPDD	NCvsPDD	MCIvsHC	NCvsHC	PDDvsHC
Age(years)	61.00 (9.50)	62.00 (13.00)	62.00 (6.00)	63.00 (5.75)	0.591	1.000	0.228	0.948	0.091	0.388
Gender(male/female)	20/25	28/22	17/14	18/22	0.261	0.919	0.373	0.300	0.959	0.411
Education(years)	12.00 (5.50)	9.50 (3.25)	9.00 (4.00)	12.00 (5.50)	1.000	0.601	0.324	0.069	0.191	**0.004**[a]
Duration(years)	5.00 (5.50)	3.00 (4.00)	5.00 (4.00)	–	0.104	0.132	0.472	–	–	–
HY	2.00 (0.75)	2.00 (0.63)	2.00 (1.50)	–	0.230	1.000	0.306	–	–	–
MDS-UPDRSIII	16.00 (17.50)	25.75 (21.5)	35.00 (11.00)	–	0.804	0.132	0.387	–	–	–
MMSE	29.00 (1.25)	29.00 (2.25)	19.00 (5.00)	29.00 (2.00)	0.661	**3.53e-11**[a]	**3.43e-14**[a]	0.145	1.000	**1.80e-15**[a]
MoCa	27.00 (2.00)	24.00 (2.00)	15.00 (5.00)	27.00 (2.00)	**3.49e-10**[a]	**4.24e-04**[a]	**1.63e-20**[a]	**1.45e-11**[a]	1.000	**7.78e-22**[a]
Attention	−0.40 (0.22)	−0.62 (0.46)	−1.43 (0.61)	−0.08 (0.89)	**0.014**[a]	**5.18e-05**[a]	**1.46e-9**[a]	**8.98e-04**[a]	0.949	**9.69e-11**[a]
Execution	−1.37 (0.20)	−1.78 (0.87)	−2.86 (0.88)	−0.07 (0.34)	**0.004**[a]	**1.55e-04**[a]	**7.84e-10**[a]	**3.94e-08**[a]	**0.030**[a]	**2.59e-16**[a]
Language	−1.35 (0.25)	−1.80 (0.50)	−2.34 (0.56)	−0.04 (0.90)	**4.84e-04**[a]	**8.42e-05**[a]	**9.97e-12**[a]	**2.31e-07**[a]	0.200	**1.10e-15**[a]
Memory	−2.41 (0.23)	−3.01 (0.35) −1.36 (0.47)	−3.86 (0.54)	0.03 (1.06)	**1.42e-04**[a]	**6.28e-05**[a]	**9.86e-13**[a]	**1.67e-08**[a]	0.134	**2.11e-17**[a]
Visuospatial	−1.03 (0.35)		−2.08 (0.36)	0.06 (0.73)	**0.031**[a]	**8.27e-05**[a]	**1.12e-08**[a]	**1.19e-07**[a]	0.115	**4.36e-16**[a]
LEDD	337.50 (412.50)	300.00 (362.50)	450.00 (380.00)	–	1.000	0.839	1.000	–	–	–

Continuous variables distributed non-normally are expressed as median(interquartile range-IQR), whilst categorical variable is presented with number of patients.
HC healthy controls, *NC* normal cognitive, *MCI* mild cognitive impairment, *PDD* Parkinson's disease dementia, *MoCa* Montreal Cognitive Assessment, *HY* Hoehn and Yahr stage, *MDS-UPDRSIII* the part III of the Movement Disorder Society-Sponsored Revision of the Unified Parkinson's Disease Rating Scale, *LEED* levodopa equivalent dose, *a* indicates significant results of post hoc Dunn's tests with Bonferroni correction.
The bold value indicates significant results of post hoc Dunn's tests with Bonferroni correction.

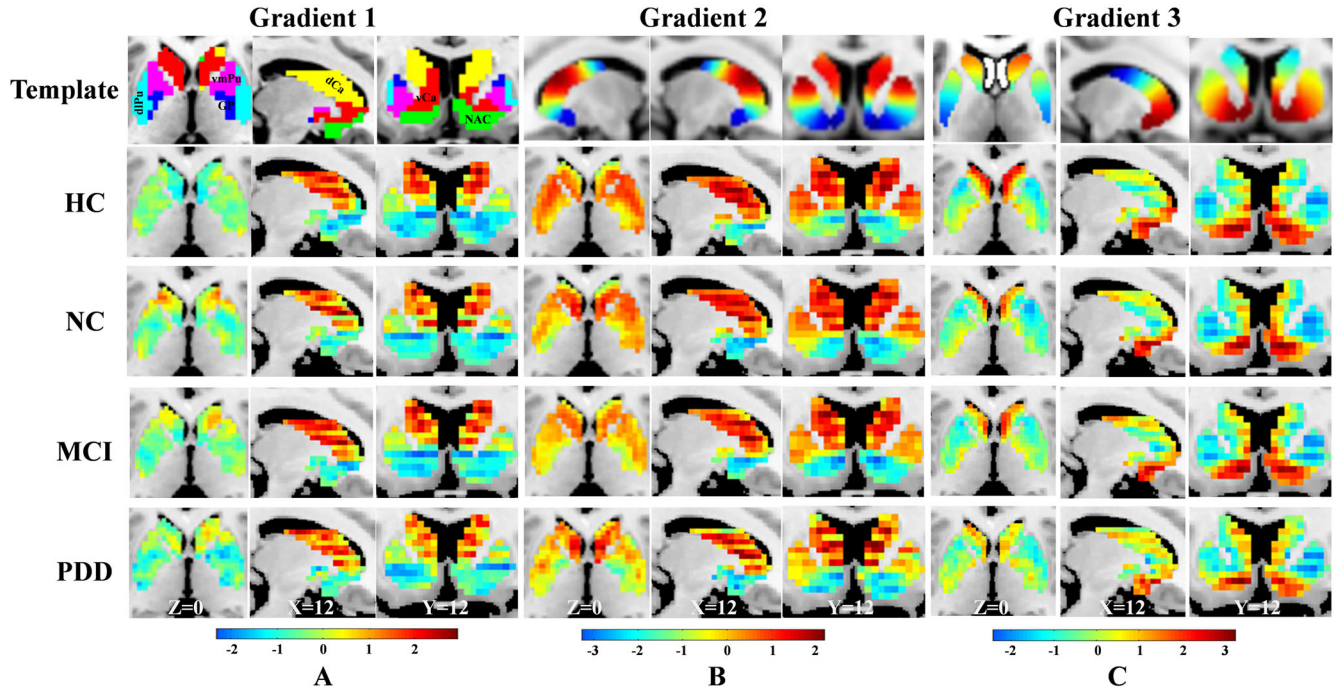

Fig. 2 | The distribution of the first three striatal functional connectivity gradients. The template for Gradient 1, derived from the Human Brainnetome Atlas, reflects the anatomical subdivisions of the striatum. Based on previous studies[1], the templates for Gradient 2 and Gradient 3 correspond to striatal gradients associated with dopaminergic projections and cortico-striatal connectivity, respectively. HC healthy controls, NC normal cognitive, MCI mild cognitive impairment, PDD Parkinson's disease dementia.

Table 2 | Group-related difference in global gradient measurements

	Variables	PD-NC	PD-MCI	PDD	HC	*F*	*P*
Gradient1	Explanatory rate	0.179 ± 0.033	0.183 ± 0.035	0.191 ± 0.035	0.176 ± 0.032	0.896	0.445
	Range	0.171 ± 0.041	0.168 ± 0.037	0.167 ± 0.035	0.165 ± 0.028	0.227	0.878
	Variability	0.042 ± 0.014	0.042 ± 0.013	0.041 ± 0.013	0.041 ± 0.009	0.136	0.938
Gradient2	Explanatory rate	0.123 ± 0.015	0.124 ± 0.018	0.113 ± 0.010	0.121 ± 0.014	2.599	0.055
	Range	0.194 ± 0.043	0.201 ± 0.051	0.211 ± 0.047	0.193 ± 0.040	0.786	0.504
	Variability	0.048 ± 0.015	0.051 ± 0.018	0.055 ± 0.018	0.049 ± 0.014	0.995	0.397
Gradient3	Explanatory rate	0.093 ± 0.016	0.094 ± 0.014	0.092 ± 0.015	0.094 ± 0.011	0.167	0.919
	Range	0.165 ± 0.034	0.162 ± 0.034	0.156 ± 0.032	0.168 ± 0.029	0.697	0.555
	Variability	0.039 ± 0.012	0.039 ± 0.011	0.037 ± 0.010	0.040 ± 0.011	0.506	0.679

The variables are expressed as mean ± Standard Deviation.
HC healthy controls, *PD-NC* Normal cognitive, *PD-MCI* mild cognitive impairment, *PDD* Parkinson's disease dementia.

gradient scores in the bilateral dorsal caudate (dCa) and lower scores in the bilateral NAC compared to PD-NC patients. Compared to PD-MCI patients, PDD patients exhibited higher gradient scores in the right ventral caudate (vCa.R) and left dorsal caudate (dCa.L), along with lower scores in the bilateral NAC. After controlling for covariates, Gradient 3 scores in the NAC.R were positively correlated with executive function ($r = 0.249$, $P = 0.019$) and language ($r = 0.240$, $P = 0.025$) sub-scores in PD patients (Supplementary Fig. S3). Compared to HC, PDD patients demonstrated lower Gradient 3 scores in the vCa.R.

The Gradient 2 is similar with the previously reported second-order connectivity mode, which demonstrated a strong correlation with DAT SPECT imaging ($r = 0.884$)[30], we further investigated the effect of medication on gradient scores by analyzing inter-group differences without considering LEDD as a covariate. In this analysis, PD-MCI patients showed lower gradient scores in the NAC.R compared to PDD patients and higher gradient scores in the right dorsolateral putamen compared to PD-NC patients (Table 3).

Due to the lateralized dominance of PD, the side of predominant nigrostriatal dopamine depletion is likely to affect striatal connectivity patterns. To examine the impact of different dominant sides on dopamine-related Gradient 2, we divided PD patients into left-dominant and right-dominant groups (Supplementary Table S1). No significant differences in Gradient 2 were observed between the left-dominant and right-dominant groups.

Network-level analyzes revealed significant differences in Gradient 3 scores within the limbic network and DMN across the four groups ($F = 4.451$, $P = 0.005$; $F = 4.686$, $P = 0.004$, respectively). Specifically, PDD patients exhibited higher Gradient 3 scores in the limbic network compared to PD-MCI patients (ΔMean = 0.198, $P = 0.024$, Bonferroni corrected) and HCs (ΔMean = 0.255, $P = 0.004$, Bonferroni corrected). Additionally, PDD patients had lower Gradient 3 scores in the DMN compared to HCs (ΔMean = −0.123, $P = 0.004$, Bonferroni corrected). No significant differences were observed in other networks among the four groups ($P > 0.05$, Bonferroni corrected).

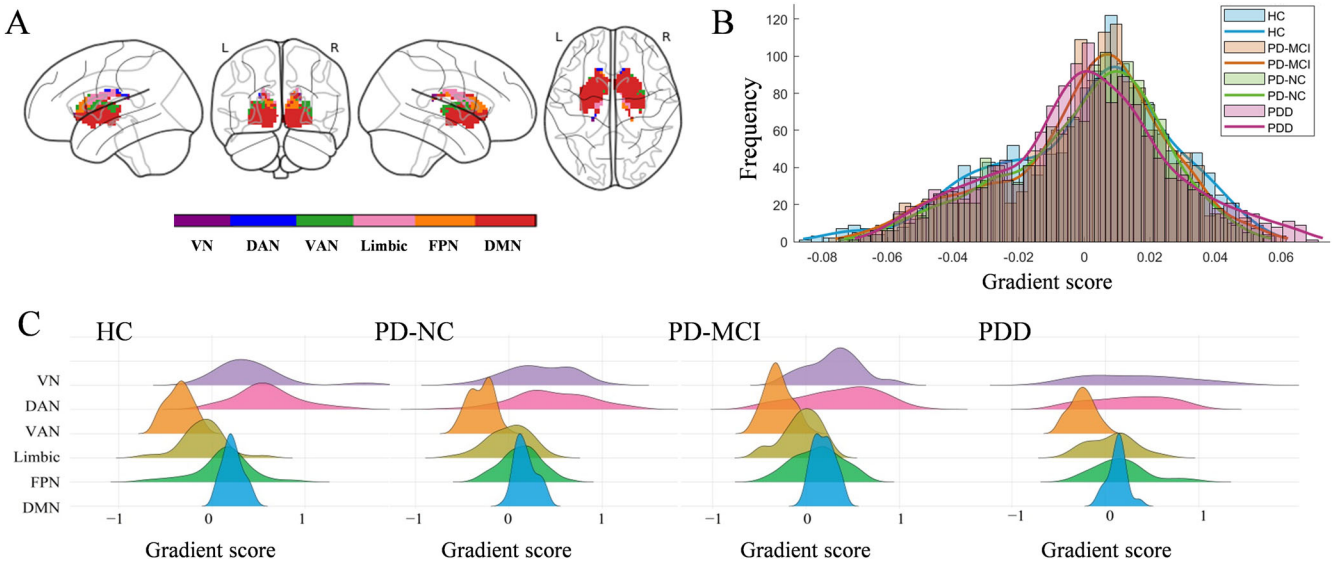

Fig. 3 | The distribution of Gradient 3 and its relationships with functional networks. A The distribution of the striatum functional atlas, created using a custom winner-take-all parcellation method. **B** The global histogram of Gradient 3 showed that the extreme values at both ends in all PD subgroups were suppressed compared to HC. **C** The distributions of the gradient scores within the striatum for each subgroup mapped to the Yeo-7 network parcellation. HC healthy controls, PD-NC normal cognitive, PD-MCI mild cognitive impairment, PDD Parkinson's disease dementia, VN visual network, DAN dorsal attention network, VAN ventral attention network, FPN frontoparietal network, DMN default mode network.

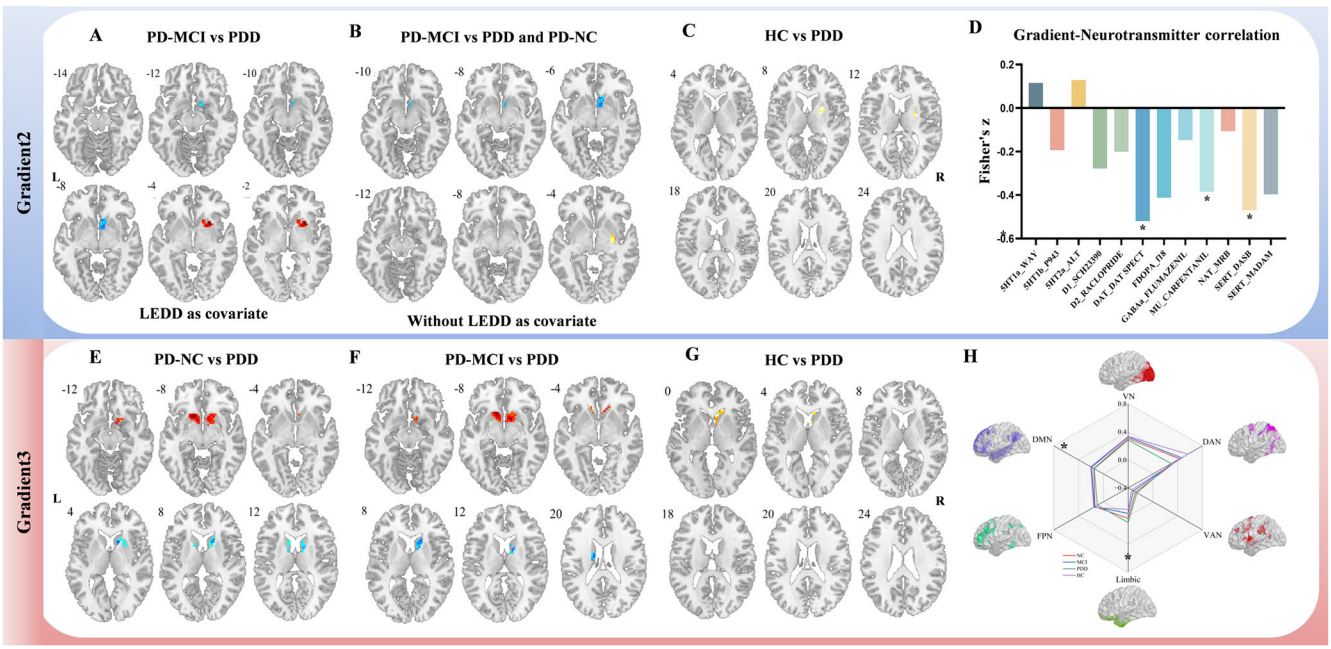

Fig. 4 | The voxel-level and network-level group-related differences in stratial gradient. A: Voxel-level group-related differences in Gradient 2 between PD-MCI and PDD patients with LEDD as covariate. **B**, **C**: Voxel-level group-related differences in Gradient 2 between PD-MCI and PDD, and between PD-MCI and PD-NC patients, respectively, without adjusting for LEDD. **D**: Correlation between Gradient 2 and the neurotransmitter atlas, with the mean Gradient 2 map showing significant spatial correspondence with DAT, MU_CARFENTANIL, and SERT_DASB distributions. **E**–**G**: Voxel-level group-related difference in Gradient 3 between PD-NC and PDD, between PD-MCI and PDD, and between HC and PDD, respectively. **H**: Network-level group-related differences in gradient scores. HC healthy controls, PD-NC normal cognitive, PD-MCI mild cognitive impairment, PDD Parkinson's disease dementia, L left, R right.

Gradient-neurotransmitter correlation analysis

The mean Gradient 2 map exhibited significant spatial correspondence with the distribution of DAT, MU_CARFENTANIL, and SERT_DASB markers ($Z = 0.520$, $P = 9.99e\text{-}05$; $Z = 0.385$, $P = 9.99e\text{-}05$; $Z = 0.469$, $P = 9.99e\text{-}05$) (Fig. 4). Although correlations were observed with other neurotransmitter distributions, the correlation with DAT SPECT scans was higher than any other PET/SPECT markers.

Potential molecular mechanism underlying striatal gradient alterations

Gradient 3 exhibited significant differences in both the PD-MCI and PDD stages. Therefore, this study primarily investigates the molecular mechanisms underlying these differences in Gradient 3. In the comparison between PD-NC and PDD patients, the second component of the PLS regression (PLS2) explained 28.5% of the variance ($P < 0.001$, permutation test) and

Table 3 | Voxel-level group-related alteration in striatum gradient

Brain regions	Cluster size	Peak coordinates			*T* value	*P* value
	(voxels)	X	Y	Z		
Gradient2						
PD-MCIvsPDD						
dorsolateral Putamen.R	15	27	12	−3	5.572	**0.019***
Nucleus accumbens.R	16	9	9	−6	−4.715	**0.003***
Without LEDD						
PD-MCIvsPDD						
Nucleus accumbens.R	14	6	15	−6	−4.390	**0.036***
PD-MCIvsPD-NC						
dorsolateral Putamen.R	13	30	−9	−3	4.720	**0.014***
Gradient3						
PD-NCvsPDD						
Nucleus accumbens.L	36	−12	15	−9	7.424	**<0.001***
Nucleus accumbens.R	42	12	9	−9	7.564	**<0.001***
dorsal Caudate.L	12	−15	-6	21	−6.048	**0.003***
dorsal Caudate.R	29	18	18	9	−5.656	**<0.001***
PD-MCIvsPDD						
Nucleus accumbens.L	38	−12	15	−9	6.839	**<0.001***
Nucleus accumbens.R	33	12	9	-9	4.922	**<0.001***
ventral Caudate.R	50	12	15	3	−6.651	**<0.001***
dorsal Caudate.L	15	−12	0	12	−4.489	**0.001***
PDDvsHC						
ventral Caudate.R	20	9	21	0	−4.745	**0.048***

The negative *t* value represents lower gradient scores and the positive *t* value represents higher gradient scores. *P* value: FDR corrected.
MNI Montreal Neurological Institute; x, y, z are the coordinates of primary peak locations in the MNI space, *HC* healthy controls, *NC* Normal cognitive, *MCI* mild cognitive impairment, *PDD* Parkinson's disease dementia, *L* left, *R* right, * Indicates statistical significance.

showed a positive correlation with T-maps (PD-NC vs PDD) (r = 0.533, $P < 0.001$, permutation test). Genes with positive weights (801 genes) were significantly enriched in GO biological processes such as "intracellular protein transport", "import into cell", "membrane organization", and "proteolysis involved in protein catabolic process". These genes were also enriched in KEGG pathways including "Mitophagy–animal" and "Parkinson's disease". Conversely, genes with negative weights (576 genes) were enriched in GO biological processes related to "regulation of membrane potential", "brain development", and "kidney development", and were significantly represented in the KEGG pathway for the "cAMP signaling pathway" (Fig. 5A).

When comparing patients with PD-MCI to those with PDD, PLS2 explained 30.2% of the variance (permutation test, $P < 0.001$) and was positively correlated with T-maps (PD-MCI vs PDD) (Pearson's $r = 0.549$, permutation test, $P < 0.001$). Positive weight genes (361 genes) were significantly enriched in GO biological processes such as "import into cell", "calcium-ion regulated exocytosis", and "membrane organization". These genes were also enriched in the KEGG pathway for "Phagosome". Negative weight genes (208 genes) were enriched in GO biological processes including "tube morphogenesis", "chromatin remodeling", and "negative regulation of protein modification process", and were significantly represented in the KEGG pathways for "Rap1 signaling pathway" and "Adherens junction" (Fig. 5B).

In the comparison between HC and PDD patients, the first components of the PLS regression (PLS1) explained 14.4% of the variance (permutation test, $P < 0.001$) and showed a positive correlation with T-maps (HC vs PDD) (Pearson's $r = 0.379$, permutation test, $P < 0.001$). Positive weight genes (122 genes) were enriched in GO biological processes such as "oligodendrocyte differentiation", "neuron projection development", and "cellular component assembly involved in morphogenesis". These genes were also enriched in the KEGG pathway for "Ether lipid metabolism". Negative weight genes (25 genes) were enriched in biological processes related to the "purine ribonucleotide catabolic process" and "export from cell" (Fig. 5C).

Validation analysis

The demographic data are provided in Supplementary Table. S2. The average striatal connectivity gradients of PD patients in the PPMI database are shown in Supplementary Fig. S4 and demonstrate a high degree of concordance with the striatal functional connectivity gradients observed in our study. Specifically, the correlations for the average gradients were as follows: Gradient 1, $r = 0.7217$, $P < 3.46E\text{-}5$; Gradient 2, $r = 0.6469$, $P < 3.46E\text{-}5$; and Gradient 3, $r = 0.7891$, $P < 3.46E\text{-}5$.

Discussion

This study is the first to evaluate the striatum gradient and its potential genetic expression associations in PD patients with continuous cognitive decline. Specifically, Gradient 1 of the striatum is partially aligns with known striatal subdivisions, which remain stable throughout disease progression. The Gradient 2 captures a spatial continuum closely linked to dopaminergic innervation of the striatum, and appears prominent primarily in dementia stage. The Gradient 3 maps onto cortico-striatal connectivity patterning and is relevant to both mild and severity cognitive impairment in PD. Remarkably, further transcription-neuroimaging spatial correlation analysis established a link between cortico-striatal gradient alterations and gene expression.

The striatum, with its extensive cortical connections, is increasingly recognized as a central hub for functional integration, particularly in PD[31,39]. Traditional methods for assessing connectivity between predefined striatal

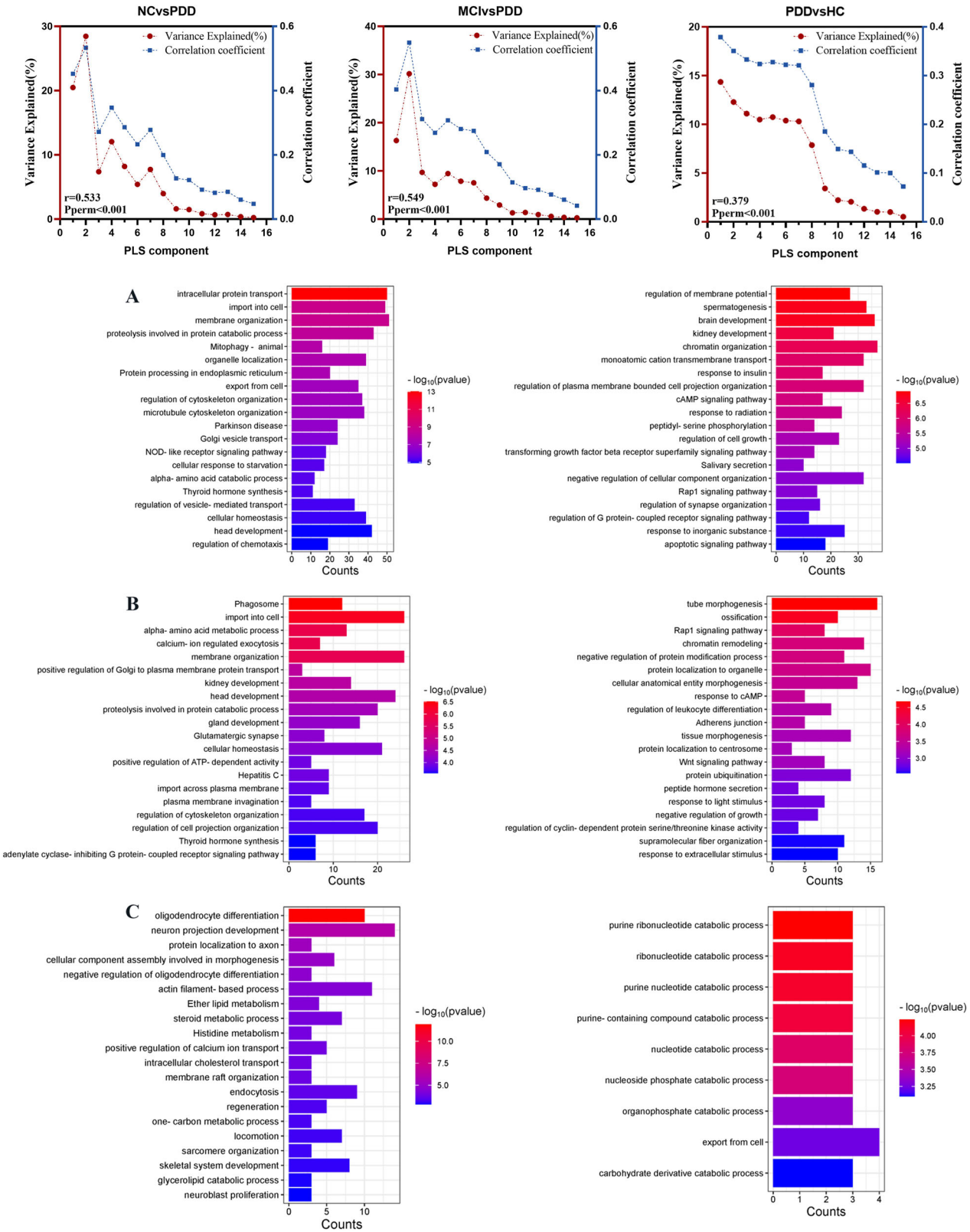

Fig. 5 | The potential molecular mechanisms of group-related striatalal gradient alterations. The top panel shows the explained ratios (left vertical axis) and correlation coefficients (right vertical axis) for the first 15 components obtained from PLS regression analysis. **A** The top 20 enriched terms that remained significant after FDR correction for positive weight (left) and negative weight (right) gene sets associated with striatum gradient differences between PD-NC and PDD patients. **B** The top 20 enriched terms that remained significant after FDR correction for positive weight (left) and negative weight (right) gene sets associated with striatum gradient differences between PD-MCI and PDD patients. **C** The top 20 enriched terms that remained significant after FDR correction for positive weight (left) and negative weight (right) gene sets associated with striatal striatum differences between PDD patients and HC. In (**A**–**C**) the length of the bar denotes the number of input genes falling under that term, and its color denotes the enrichment significance.

regions and the cortex often rely on hard parcellations[6], which may fail to capture the overlapping functional roles and diverse cortical projections of striatal subregions. Our study reveals that the Gradient 1 of the striatum demonstrates continuous spatial variation across its anatomical subdivisions—from the caudate to the putamen and nucleus accumbens. It partially corresponds to these subdivisions while also uncovering multiple overlapping functional connectivity patterns within these regions. Importantly, this gradient pattern was validated using the PPMI database, exhibiting a high correlation with the pattern observed in our local dataset. Notably, there were no significant differences in Gradient 1 scores between disease groups or across various stages of cognitive impairment in PD, suggesting that Gradient 1 remains relatively stable despite the onset and progression of the disease. Although large-scale studies, such as the HCP, have demonstrated anatomically specific gradient connectivity[40], these findings are preliminary and based on hypotheses derived from studies with limited sample sizes and lacking longitudinal data.

The Gradient 2 indicates that the dorsal putamen and dorsal caudate share similar functional characteristics, which are distinct from those of the ventral putamen and ventral caudate. Pathophysiological studies have shown that the ventral and dorsal striatum receive dense dopaminergic projections from the ventral tegmental area (VTA) and substantia nigra (SN), respectively[41]. Gradient 2 may reflect a functional-anatomical gradient shaped by the distinct influences of these dopaminergic systems on striatal subregions. Furthermore, our neurotransmitter atlas correlation analysis for Gradient 2 revealed that this striatal connectivity pattern closely corresponds to dopamine transporter (DAT) availability in the striatum. Although no publicly available dataset currently provides both high-resolution resting-state fMRI and DAT SPECT scans from the same participants, this alignment further suggests that the mesolimbic and nigrostriatal dopaminergic gradients projecting to the striatum, as observed in tract-tracing studies in rodents and non-human primates[31]. Similar observations were reported by Marianne Oldehinkel et al., who demonstrated a strong correlation between this striatal connectivity pattern and DAT SPECT imaging across both the HCP and PPMI databases[30]. Moreover, Elior Drori et al. indicated that alterations in the striatum are intricately linked to the pathophysiology of PD, with abnormalities in the putamen's gradient in PD patients potentially reflecting the dopaminergic deficits underlying motor dysfunction[29]. Overall, our findings are consistent with existing research, highlighting the presence of a dopamine transporter (DAT) density gradient in the striatum and its potential role in the clinical manifestations of PD.

After controlling for LEDD, our group analysis revealed that PDD patients showed higher gradient scores in the right nucleus accumbens and lower scores in the right dorsolateral putamen compared to PD-MCI patients. In addition, all PD subgroups exhibited lower gradient scores in both dorsal and ventral striatal regions than HCs. In PD patients, a decrease in dorsal regions and an increase in ventral regions indicate shifts in a region's position along the gradient continuum. These findings imply potential alterations in dopaminergic innervation within the striatum, characterized by a relative decrease in dopaminergic input to both dorsal and ventral striatal areas. Furthermore, gradient scores in the right nucleus accumbens were negatively correlated with global cognitive performance and memory dominance. This indicates that higher ventral gradient values, reflecting a more pronounced disruption of the Gradient 2 continuum, may be more pronounced in the advanced stages of the illness[42]. When LEDD was not controlled for, PD-MCI patients exhibited higher gradient scores in the right dorsolateral putamen compared to PD-NC patients. This finding supports the hypothesis that gradient continuum changes in the striatum are influenced by dopaminergic medications, with the putamen showing heightened sensitivity to dopamine alterations compared to other striatal nuclei[28,30]. However, regardless of LEDD adjustment, no statistically significant differences were found in PD patients based on the affected sides. This unexpected result may reflect the influence of LEDD medications, despite efforts to control for their effects, and suggests that the long-term impact of these medications cannot be entirely ruled out.

Gradient 3 presents as a ventromedial-to-dorsolateral gradient, reflecting the topographic organization of cortico-striatal connectivity. In contrast to the preceding gradients, disruptions in dorsolateral striatal-cortical connectivity are clinically associated with cognitive impairments in PD, affecting both mild and severe stages of cognitive decline. Significant voxel-level group differences in Gradient 3 were observed: PDD patients exhibited lower gradient values in the ventromedial striatum and higher values in the dorsolateral caudate compared to other groups. The worsening cognitive function observed in PDD appears to result from interactions within the striatum-cortical loops. Prior studies have reported that cognitive performance is associated with reduced functional connectivity within the dorsal circuit and increased connectivity within the ventral circuit[29,43]. The positive correlation between Gradient 3 scores in the right nucleus accumbens and visuospatial sub-scores in our study further supports the idea that decreased functional activity within the ventral circuit contributes to cognitive decline.

Previous studies have investigated cortical-striatal connectivity patterns, but limitations in analysis algorithms have hindered precise localization of striatal connections to the cortex. Our study, utilizing network-based analysis, identified that the functional subdivisions of the striatum align with six canonical networks and are hierarchically distributed along a dominant gradient. Specifically, these subdivisions range from the DAN and VN at one extreme to the VAN at the opposite end of Gradient 3. The relationship between striatal structure and function, in both health and disease, likely depends on its position within the cortical hierarchy[29]. Our network cortical localization analysis demonstrated substantial and coherent overlap between regions connected to DAN and VN. This coexistence of clearly segregated as well as overlapping connections from cortical sites to striatal subregions reflects the presence of both parallel and integrative networks within the striatum[32]. Group comparisons revealed that gradient scores for the limbic network (located in the bilateral dorsal caudate) were significantly higher in PDD compared to HC and PD-MCI groups, while gradient scores for the DMN, which includes the bilateral ventral caudate, nucleus accumbens, and ventromedial putamen, were lower. These findings not only achieve precise localization of striatal regions' connectivity to the cortex but also further support the notion that increased gradient scores in the dorsal striatum may contribute to cognitive decline, potentially associated with changes in limbic network projections. Conversely, the heightened connectivity between the DMN and the ventral striatum appears to be involved in maintaining cognitive functions.

Furthermore, transcriptome–connectome association analysis revealed that alterations in the macroscale striatal gradient in PDD are linked to microscale transcriptomic architectures. Specifically, genes associated with gradient changes in PDD, when compared to PD-NC and PD-MCI groups, were enriched in processes related to transport, membrane organization, and protein/amino acid metabolism (PLS+), as well as in development-related and cell projection-related processes (PLS-). KEGG pathway analysis showed enrichment in phagosome, protein processing in the endoplasmic reticulum, Parkinson's disease (PLS+), and Rap1 and cAMP signaling pathways (PLS−). This finding is not surprising, given that the typical pathophysiological basis of PD involves protein folding and transport damage. Furthermore, compared to HCs, genes associated with Gradient 3 alteration in PDD were enriched in pathways related to oligodendrocyte differentiation (PLS+). This finding aligns with previous studies, as emerging evidence suggests that oligodendrocyte dysfunction may play a critical role in white matter loss in PD dementia[44]. Additionally, studies have reported that PD patients with visual impairment and dementia exhibit higher oligodendrocyte density in brain tissues[36]. Therefore, our findings provide preliminary evidence that oligodendrocyte-associated genes may contribute to the cognitive deficits observed in PD.

Several limitations should be acknowledged in this study. First, it is a cross-sectional study, and longitudinal studies tracking gradient changes over the course of cognitive decline could provide more insightful implications. Second, the relatively small sample size, particularly for the PDD group, may limit the generalizability of our findings. Third, the observed

association between striatal gradient and transcriptome profiles is preliminary because the gene transcription data were obtained from healthy donors. Future studies should incorporate larger samples of whole-brain gene expression data from PD patients to validate the connectome-transcriptome relationship. Finally, due to the lack of prior quantitative assessments, the similarity between Gradient 2 in our study and the previously reported second-order connectivity pattern remains descriptive. Additionally, the correlations between neurotransmitter gradients were derived from atlas-based PET data rather than direct imaging measures. PET-fMRI studies are essential for confirming the direct association between gradient connectivity patterns and dopaminergic function, highlighting a critical direction for future research.

Methods

Participants

Between February 2019 and April 2024, the Neurology Clinic at the First Hospital of China Medical University enrolled 138 patients diagnosed with PD (PD-NC, $n = 49$; PD-MCI, $n = 55$; PDD, $n = 34$). Diagnosis was confirmed by experienced neurologists according to the criteria established by the United Kingdom Parkinson's Disease Society Brain Bank[45]. During this period, a control group of 41 age- and gender-matched healthy individuals was also recruited. This control group underwent the same MRI techniques and cognitive assessments as the PD patient group. All patients were off antiparkinsonian medications for at least 12 h before the MR scans and cognitive assessments. The study protocol was approved by the ethical council of the First Hospital of China Medical University, and all participants provided informed written consent before their inclusion in the study.

Clinical assessment

Participant demographic information, including personal details such as age, gender, education level for all individuals, disease duration, and daily Levodopa equivalent dosage (LEDD) for PD patients, was carefully recorded. To evaluate motor disability related to PD, we employed the Movement Disorder Society-Sponsored Revision of the Unified Parkinson's Disease Rating Scale (MDS-UPDRS), with particular emphasis on its third section (MDS-UPDRS III)[46], along with the Hoehn and Yahr (HY) scales. Global cognitive function was assessed using the Mini-Mental State Examination (MMSE) and Montreal Cognitive Assessment (MoCA).

Patients were classified into cognitive subgroups according to the Movement Disorder Society (MDS) Task Force guidelines, each PD participant completed at least two tests within each of the following five cognitive domains: Attention: (1) Trail Making Test-A (TMT-A), (2) Digit Ordering, (3) Symbol Digit Modalities Test (SDMT) ; Executive Function: (1) Stroop Color-Word Interference Test (CWT), (2) 10-Point Clock Drawing Test; Language: (1) Boston Naming Test, (2) Category Fluency (animals), (3) Verbal Fluency Test (letter); Memory: (1) Rey Auditory Verbal Learning Test (RAVLT), (2) Brief Visuospatial Memory Test-Revised (BVMT-R); Visuospatial Function: (1) Clock Copying test, (2) Complex Figure Test (CFT). Additionally, functional impairment[47] was assessed by consulting the patients and their caregivers.

The raw cognitive domain scores were adjusted for age, education level, and gender. Subsequently, *Z*-score normalization was applied to each cognitive domain score using the mean and standard deviation of the healthy control group. Domain scores for each participant were then calculated by averaging the individual test *Z*-scores within each domain. PD participants were classified as PD-MCI if they scored at least 1.5 standard deviations (SD) below the mean on a minimum of one test in two cognitive domains, or two tests in one cognitive domain, without functional impairment[47,48]. If cognitive impairment was accompanied by functional impairment, the participants were classified as PDD. All other participants were classified as PD-NC.

MRI acquisition and processing

All participants underwent MRI scanning on a 3.0 T Magnetom Verio scanner (Siemens, Erlangen, Germany) equipped with a 32-channel head coil. High-resolution three-dimensional T1-weighted images and rs-fMRI sequences were acquired using a standardized protocol, with detailed acquisition parameters provided in Supplementary Note 2. The rs-fMRI data were preprocessed using Gretna software (Gretna V2.0.0, https://www.nitrc.org/projects/gretna) in Matlab R2020b. The pipeline included: (i) discarding the first 10 time points; (ii) slice timing correction; (iii) motion correction, excluding participants with head motion exceeding 2 mm translation or 2° rotation in any direction, and computing frame-wise displacement (FD) to assess volume-to-volume motion. Based on these criteria, 4 PD-NC, 5 PD-MCI, 3 PDD patients, and 1 HC were excluded; (iv) spatial normalization to the standard Montreal Neurological Institute (MNI) space using the Dartel method; (v) regression of nuisance covariates, including the Friston-24 model, spike volumes (FD > 0.5 mm), white matter, and cerebrospinal fluid signals; (vi) band-pass filtering (0.01–0.08 Hz). After preprocessing, 45 PD-NC, 50 PD-MCI, 31 PDD patients, and 40 HCs were included in the analysis.

Construction of the connectome gradient maps

The striatal connectivity gradients were constructed using MATLAB scripts following and colleagues[26]. The Human Brainnetome Atlas was used to define key striatal regions, encompassing 1,447 voxels across key regions, including the ventral caudate (vCa), globus pallidus (GP), nucleus accumbens (NAC), ventromedial putamen (vmPu), dorsal caudate (dCa), and dorsolateral putamen (dlPu). Individual BOLD time courses were extracted and z-scored, and a voxel-wise striatum-to-cerebrum functional connectivity matrix ($1447 \times 39{,}976$) was generated using Pearson's correlations, excluding intra-striatal connections. Fisher's *Z*-transformation was applied to improve normality, and only the top 10% of connections per row were retained[49,50]. A symmetric affinity matrix was then constructed using cosine distance to reflect connectivity similarity. The diffusion map embedding algorithm, implemented in BrainSpace (a MATLAB toolbox: https://github.com/MICA-MNI/BrainSpace)[51], was used to compute principal gradients, with α set to 0.5[26,50,52] for optimal connectivity mapping. Gradient values were assigned to each voxel within the striatum, forming a topographical gradient map. Gradients were aligned to a group template via Procrustes rotation[53], and group-level maps were obtained by averaging individual gradients. To assess gradient stability across disease stages, voxel-wise spatial correlations were computed between subgroup mean maps (HC, PD-NC, PD-MCI, PDD), with Bonferroni correction applied ($P < 0.05/1447$).

Global gradient measurements

Three global gradient measurements, namely, gradient range, variability and explanatory rate, are calculated. The definitions of these gradient measurements are provided in Supplementary Note 3.

Relevance to functional networks

To map functional correlates of striatal gradients, we integrated the Yeo-seven-network parcellation[54] with a data-driven striatal atlas. Employing a validated winner-take-all approach[26,55], we computed functional connectivity between each striatal voxel's BOLD signal and canonical cortical networks. Voxels were assigned to the network demonstrating maximal temporal correlation, generating a striatal functional atlas comprising seven subdivisions aligned with macroscale brain networks.

Voxel-level and network-level group-related difference in striatal gradient

Two-sample *t*-tests were employed in SPM12 to assess voxel-wise group differences in gradient scores between each PD subgroup and the HC group, controlling for age, sex, years of education, and frame-wise displacement (FD). For comparisons among PD subgroups, a one-way ANOVA was conducted with additional covariates for LEDD and disease duration. Pairwise differences among PD subgroups were further assessed through post hoc analyses. FDR correction was applied for multiple comparisons in

two-sample *t*-tests, ANOVA, and post hoc analyses, with statistical significance set at $P < 0.05$.

Based on the 'Relevance to functional networks' results, we extracted the mean gradient values of voxels corresponding to the Yeo-7 network parcellation within each striatal functional network subdivision. GLM analyses were employed to compare group differences in network-level scores, using the same covariates as mentioned earlier. The significance level was set at $P < 0.05$, and multiple comparisons were corrected using the Bonferroni method.

Gradient-neurotransmitter correlation analysis

Previous studies have demonstrated a strong correlation between Gradient 2 connectivity patterns and DAT SPECT imaging ($r = 0.884$)[30]. To further investigate the spatial correspondence of the Gradient 2 to DAT SPECT relative to other PET/SPECT scans targeting various neurotransmitter systems, we conducted an analysis of the spatial correspondence between Gradient2 and multiple PET/SPECT markers. These PET/SPECT markers, which reflect different neuromodulatory systems, were obtained from the publicly available JuSpace toolbox (https://github.com/juryxy/JuSpace)[56], with details provided in Supplementary Note 4. Pearson correlation coefficients were computed between mean gradient scores and neurotransmitter maps, with results normalized using Fisher's *r*-to-*z* transformation. Absolute correlation values were used for interpretation. To validate the significance of the observed correlations, exact permutation-based *p* values were calculated using permutation testing ($N = 10000$). More specifically, we created randomly permuted surrogate PET/SPECT maps and thereby generated a null distribution[57] by computing the absolute (Fisher *r*-to-*z* normalized) correlations between the mean Gradient 2 map and the permuted PET/SPECT maps[30]. Additionally, using this null distribution, we defined a Bonferroni-corrected threshold for significance at $p = 0.0008$ (i.e., $p = 0.01/12$ PET and SPECT scans), which was included in the top figure showing the correlations with the other PET tracers[30].

Genetic architecture underlying the gradient alterations

Brain gene expression data were obtained from the AHBA dataset (http://www.brainmap.org)[58], which was derived from six human post-mortem donors. The original expression data of brain tissue samples were processed with the abagen toolbox using a newly proposed pipeline(https://www.github.com/netneurolab/abagen)[40]. After brain gene expression data processing, we obtained normalized expression data of 15,633 genes for 134 tissue samples within the striatum, yielding a final sample × gene matrix of 134 × 15,633.

Partial least squares regression (PLS) was employed to investigate the relationship between voxel-wise statistical parametric maps derived from two-sample *t*-tests comparing striatal gradient scores between groups (represented by T-maps) and the transcriptional activity of 15,633 genes. The the gene expression matrix served as the independent variables, while the *t*-value maps were treated as the dependent variables. To account for the spatial autocorrelation (SA) inherent in brain maps, spin permutation testing based on 5000 spherical rotations of the t-value map was conducted to evaluate the null hypothesis that the second PLS component (PLS2) explained more covariance between the gradient alterations and whole-genome expression than would be expected by chance[59]. Additionally, gene weights were converted into *z*-scores by dividing by the standard deviation of the weights estimated from bootstrapping, and all genes were ranked accordingly[60]. *Z*-scores quantified each gene's contribution to the PLS regression component. Based on prior studies, genes with *z*-scores > 5 or <−5 were considered significant and classified into positive weight (PLS+) or negative weight (PLS-) gene lists, respectively[61]. This analysis was conducted using MATLAB scripts, following the methodology described by Feng and colleagues[59].

Enrichment analysis

To better understand the biological significance of PLS+ and PLS- genes, functional annotations based on Gene Ontology (GO) biological process and Kyoto Encyclopedia of Genes and Genomes (KEGG) data bases was conducted by the automated meta-analysis tool Metascape (https://metascape.org/)[62]. For the above-mentioned enrichment analyses, the resulting enrichment pathways were retained for significance at False Discovery Rate (FDR) < 0.05. Briefly, enriched terms were filtered by calculating accumulative hypergeometric *p* values and enrichment factors, and then hierarchically clustered into a tree according to Kappa similarity among their gene memberships. A threshold value kappa score of 0.3 was applied to cast the tree into term clusters[59].

Validation analysis

To validate the reproducibility of striatal functional connectivity gradients, we identified 50 PD patients in the Parkinson's Progression Markers Initiative (PPMI) dataset (https://www.ppmi-info.org/access-data -specimens/download-data) who had at least one structural and functional resting-state MRI scan collected. The scanning parameters are provided in Supplementary Note 5. We repeated the aforementioned striatal functional connectivity gradient analysis and calculated the average striatal functional connectivity gradient for all PD patients. To demonstrate the similarity between the striatal functional connectivity gradients of PD patients in the PPMI database and those in our study, we calculated the correlations between the average gradient maps of PD patients from the PPMI database and the average gradient maps of all PD patients in our study. A significance level of $P < 0.05/1447$ was considered statistically significant.

Statistical analysis

Statistical analyses were conducted using SPSS 25.0 software (IBM Software Analytics, New York, NY). The Kolmogorov-Smirnov test was used to assess the normality of demographic and behavioral data. For variables violating the normality assumption, the Kruskal-Wallis test was applied, followed by post hoc Dunn's tests with Bonferroni correction to compare PD subgroups (PD-NC, PD-MCI, PDD) and HCs. Gender distribution was analyzed using the chi-square test. Partial correlation analyses were conducted to explore the association between changes in gradient scores and cognitive performance in PD patients, with age, gender, education, disease duration, and LEDD included as covariates. A significance threshold of $P < 0.05$ (two-tailed) was set for all tests.

General Linear Model (GLM) analyses were employed to compare group differences in global gradient measurements scores, using the same covariates as mentioned earlier. The significance level was set at $P < 0.05$, and corrections for multiple comparisons were applied using the Bonferroni method.

Data availability

The participants with Parkinson's disease were recruited from the First Hospital of China Medical University. However, restrictions apply to the availability of these data, as they were used under license for the present study and are not publicly accessible. Data may be available from the authors upon reasonable request. The dataset used for validation analysis is publicly available through the Parkinson's Progression Markers Initiative (PPMI) datasets(https://www.ppmi-info.org/access-data-specimens/download-data). The gene expression data supporting the findings are available from the 2010 Allen Institute for Brain Science (http://www.brainmap.org). The PET/SPECT markers used in this study can be accessed via the publicly available JuSpace toolbox (https://github.com/juryxy/JuSpace).

Code availability

The diffusion embedding code is publicly accessible in the BrainSpace toolbox (https://github.com/MICA-MNI/BrainSpace).

Abbreviations

PD	Parkinson's Disease;
NC	Normal Cognitive;
MCI	Mild Cognitive Impairment;
PDD	Parkinson's Disease Dementia;

AHBA	Allen Human Brain Atlas;
MoCA	Montreal Cognitive Assessment;
MDS-UPDRS	Movement Disorder Society-Sponsored Revision of the Unified Parkinson's Disease Rating Scale;
FD	frame-wise displacement;
PLS	Partial Least Squares Regression;
GO	Gene Ontology;
KEGG	Kyoto Encyclopedia of Genes and Genomes;
PPMI	Parkinson's Progression Markers Initiative.

Received: 26 November 2024; Accepted: 19 May 2025;
Published online: 28 May 2025

References

1. Gorges, M. et al. Longitudinal brain atrophy distribution in advanced Parkinson's disease: What makes the difference in "cognitive status" converters?. *Hum. Brain Mapp.* **41**, 1416–1434 (2020).
2. Fiorenzato, E. et al. Dynamic functional connectivity changes associated with dementia in Parkinson's disease. *Brain* **142**, 2860–2872 (2019).
3. Goldman, J. G. & Sieg, E. Cognitive impairment and dementia in Parkinson Disease. *Clin. Geriatr. Med.* **36**, 365–377 (2020).
4. Petok, J. R., Merenstein, J. L. & Bennett, I. J. Iron content affects age group differences in associative learning-related fMRI activity. *Neuroimage* **285**, 120478 (2024).
5. Redgrave, P. et al. Goal-directed and habitual control in the basal ganglia: implications for Parkinson's disease. *Nat. Rev. Neurosci.* **11**, 760–772 (2010).
6. Marquand, A. F., Haak, K. V. & Beckmann, C. F. Functional corticostriatal connection topographies predict goal directed behaviour in humans. *Nat. Hum. Behav.* **1**, 0146 (2017).
7. Yin, Z. et al. Contribution of basal ganglia activity to REM sleep disorder in Parkinson's disease. *J. Neurol. Neurosurg. Psychiatry* **95**, 947–955 (2024).
8. Wang, H. et al. Altered functional connectivity of ventral striatum subregions in de-novo Parkinson's disease with depression. *Neuroscience* **491**, 13–22 (2022).
9. Oosterwijk, C. S., Vriend, C., Berendse, H. W., van der Werf, Y. D. & van den Heuvel, O. A. Anxiety in Parkinson's disease is associated with reduced structural covariance of the striatum. *J. Affect. Disord.* **240**, 113–120 (2018).
10. Devignes, Q. et al. Resting-state functional connectivity in frontostriatal and posterior cortical subtypes in Parkinson's disease-mild cognitive impairment. *Mov. Disord.* **37**, 502–512 (2022).
11. Baggio, H. C. et al. Resting-state frontostriatal functional connectivity in Parkinson's disease-related apathy. *Mov. Disord.* **30**, 671–679 (2015).
12. Prange, S. et al. Early limbic microstructural alterations in apathy and depression in de novo Parkinson's disease. *Mov. Disord.* **34**, 1644–1654 (2019).
13. Nigro, S. et al. Apomorphine-induced reorganization of striato-frontal connectivity in patients with tremor-dominant Parkinson's disease. *Parkinsonism Relat. Disord.* **67**, 14–20 (2019).
14. Shen, B. et al. Altered putamen and cerebellum connectivity among different subtypes of Parkinson's disease. *CNS Neurosci. Ther.* **26**, 207–214 (2020).
15. Hammes, J. et al. Dopamine metabolism of the nucleus accumbens and fronto-striatal connectivity modulate impulse control. *Brain* **142**, 733–743 (2019).
16. Lang, S. et al. Mild behavioral impairment in Parkinson's disease is associated with altered corticostriatal connectivity. *Neuroimage Clin.* **26**, 102252 (2020).
17. Bloem, B. R., Okun, M. S. & Klein, C. Parkinson's disease. *Lancet***397**, 2284–2303 (2021).
18. Winer, J. R. et al. Associations between Tau, beta-amyloid, and cognition in Parkinson disease. *JAMA Neurol.* **75**, 227–235 (2018).
19. Deng, I., Corrigan, F., Zhai, G., Zhou, X. F. & Bobrovskaya, L. Lipopolysaccharide animal models of Parkinson's disease: recent progress and relevance to clinical disease. *Brain Behav. Immun. Health* **4**, 100060 (2020).
20. Bellucci, A. et al. Review: Parkinson's disease: from synaptic loss to connectome dysfunction. *Neuropathol. Appl Neurobiol.* **42**, 77–94 (2016).
21. Assous, M. Striatal cholinergic transmission. Focus on nicotinic receptors' influence in striatal circuits. *Eur. J. Neurosci.* **53**, 2421–2442 (2021).
22. Gratwicke, J., Jahanshahi, M. & Foltynie, T. Parkinson's disease dementia: a neural networks perspective. *Brain* **138**, 1454–1476 (2015).
23. Lee, D. J. et al. Nucleus basalis of Meynert neuronal activity in Parkinson's disease. *J. Neurosurg.* **132**, 574–582 (2020).
24. van der Zee, S. et al. Altered Cholinergic Innervation in De Novo Parkinson's Disease with and Without Cognitive Impairment. *Mov. Disord.* **37**, 713–723 (2022).
25. van der Zee, S., Muller, M., Kanel, P., van Laar, T. & Bohnen, N. I. Cholinergic Denervation Patterns Across Cognitive Domains in Parkinson's Disease. *Mov. Disord.* **36**, 642–650 (2021).
26. Shen, Y. et al. Functional connectivity gradients of the cingulate cortex. *Commun. Biol.* **6**, 650 (2023).
27. Politis, M. Neuroimaging in Parkinson disease: from research setting to clinical practice. *Nat. Rev. Neurol.* **10**, 708–722 (2014).
28. Kish, S. J., Shannak, K. & Hornykiewicz, O. Uneven pattern of dopamine loss in the striatum of patients with idiopathic Parkinson's disease. *Pathophysiol. Clin. Implic. N. Engl. J. Med.* **318**, 876–880 (1988).
29. Drori, E., Berman, S. & Mezer, A. A. Mapping microstructural gradients of the human striatum in normal aging and Parkinson's disease. *Sci. Adv.* **8**, eabm1971 (2022).
30. Oldehinkel, M. et al. Mapping dopaminergic projections in the human brain with resting-state fMRI. *Elife* **11**, e71846 (2022).
31. Haber, S. N. Corticostriatal circuitry. *Dialogues Clin. Neurosci.* **18**, 7–21 (2016).
32. Draganski, B. et al. Evidence for segregated and integrative connectivity patterns in the human Basal Ganglia. *J. Neurosci.* **28**, 7143–7152 (2008).
33. Ji, Y. et al. Genes associated with gray matter volume alterations in schizophrenia. *Neuroimage* **225**, 117526 (2021).
34. Keo, A. et al. Cingulate networks associated with gray matter loss in Parkinson's disease show high expression of cholinergic genes in the healthy brain. *Eur. J. Neurosci.* **53**, 3727–3739 (2021).
35. Thomas, G. E. C. et al. Regional brain iron and gene expression provide insights into neurodegeneration in Parkinson's disease. *Brain* **144**, 1787–1798 (2021).
36. Zarkali, A. et al. Differences in network controllability and regional gene expression underlie hallucinations in Parkinson's disease. *Brain* **143**, 3435–3448 (2020).
37. Wang, Y. et al. Morphometric similarity differences in drug-naive Parkinson's disease correlate with transcriptomic signatures. *CNS Neurosci. Ther.* **30**, e14680 (2024).
38. Zarkali, A. et al. Dementia risk in Parkinson's disease is associated with interhemispheric connectivity loss and determined by regional gene expression. *Neuroimage Clin.* **28**, 102470 (2020).
39. Selemon, L. D. & Goldman-Rakic, P. S. Longitudinal topography and interdigitation of corticostriatal projections in the rhesus monkey. *J. Neurosci.* **5**, 776–794 (1985).
40. Markello, R. D. et al. Standardizing workflows in imaging transcriptomics with the abagen toolbox. Elife **10**,e72129 (2021).
41. Cox, J. & Witten, I. B. Striatal circuits for reward learning and decision-making. *Nat. Rev. Neurosci.* **20**, 482–494 (2019).
42. Oldehinkel, M. et al. Gradients of striatal function in antipsychotic-free first-episode psychosis and schizotypy. *Transl. Psychiatry* **13**, 128 (2023).

43. Mestres-Misse, A., Turner, R. & Friederici, A. D. An anterior-posterior gradient of cognitive control within the dorsomedial striatum. *Neuroimage* **62**, 41–47 (2012).
44. Bryois, J. et al. Genetic identification of cell types underlying brain complex traits yields insights into the etiology of Parkinson's disease. *Nat. Genet.* **52**, 482–493 (2020).
45. Hughes, A. J., Daniel, S. E., Kilford, L. & Lees, A. J. Accuracy of clinical diagnosis of idiopathic Parkinson's disease: a clinico-pathological study of 100 cases. *J. Neurol. Neurosurg. Psychiatry* **55**, 181–184 (1992).
46. Goetz, C. G. et al. Movement Disorder Society-sponsored revision of the Unified Parkinson's Disease Rating Scale (MDS-UPDRS): scale presentation and clinimetric testing results. *Mov. Disord.* **23**, 2129–2170 (2008).
47. Wood, K. H. et al. Diffusion tensor imaging-along the perivascular-space index is associated with disease progression in Parkinson's disease. *Mov. Disord.* **39**, 1504–1513 (2024).
48. Litvan, I. et al. Diagnostic criteria for mild cognitive impairment in Parkinson's disease: Movement Disorder Society Task Force guidelines. *Mov. Disord.* **27**, 349–356 (2012).
49. Vos de Wael, R. et al. Anatomical and microstructural determinants of hippocampal subfield functional connectome embedding. *Proc. Natl. Acad. Sci. USA* **115**, 10154–10159 (2018).
50. Dong, D. et al. Compression of cerebellar functional gradients in schizophrenia. *Schizophr. Bull.* **46**, 1282–1295 (2020).
51. Vos de Wael, R. et al. BrainSpace: a toolbox for the analysis of macroscale gradients in neuroimaging and connectomics datasets. *Commun. Biol.* **3**, 103 (2020).
52. Hong, S. J. et al. Atypical functional connectome hierarchy in autism. *Nat. Commun.* **10**, 1022 (2019).
53. Zhang, Q. et al. Atypical functional connectivity hierarchy in Rolandic epilepsy. *Commun. Biol.* **6**, 704 (2023).
54. Yeo, B. T. et al. The organization of the human cerebral cortex estimated by intrinsic functional connectivity. *J. Neurophysiol.* **106**, 1125–1165 (2011).
55. Yang, S. et al. The thalamic functional gradient and its relationship to structural basis and cognitive relevance. *Neuroimage* **218**, 116960 (2020).
56. Dukart, J. et al. JuSpace: a tool for spatial correlation analyses of magnetic resonance imaging data with nuclear imaging derived neurotransmitter maps. *Hum. Brain Mapp.* **42**, 555–566 (2021).
57. Burt, J. B. et al. Hierarchy of transcriptomic specialization across human cortex captured by structural neuroimaging topography. *Nat. Neurosci.* **21**, 1251–1259 (2018).
58. Hawrylycz, M. J. et al. An anatomically comprehensive atlas of the adult human brain transcriptome. *Nature* **489**, 391–399 (2012).
59. Feng, G. et al. Longitudinal development of the human white matter structural connectome and its association with brain transcriptomic and cellular architecture. *Commun. Biol.* **6**, 1257 (2023).
60. Morgan, S. E. et al. Cortical patterning of abnormal morphometric similarity in psychosis is associated with brain expression of schizophrenia-related genes. *Proc. Natl. Acad. Sci. USA* **116**, 9604–9609 (2019).
61. Lin, S. et al. Shared and specific neurobiology in bipolar disorder and unipolar disorder: Evidence based on the connectome gradient and a transcriptome-connectome association study. *J. Affect. Disord.* **341**, 304–312 (2023).
62. Zhou, Y. et al. Metascape provides a biologist-oriented resource for the analysis of systems-level datasets. *Nat. Commun.* **10**, 1523 (2019).

Acknowledgements

This study was supported by the National Natural Science Foundation of China (grant number 82071909).

Author contributions

Author Roles (1) Research Project: A. Conception, B. Organization, C. Execution; (2) Statistical Analysis: A. Design, B. Execution, C. Review and Critique; (3) Manuscript Preparation: A. Writing of the First Draft, B. Review and Critique.LXL: 1A, 1C, 2A, 2B, 2C, 3A, 3BBST: 1C, 2B, 2C, 3BPHZ: 1C, 2B, 2C, 3BYHM: 1A, 2C, 3BZMW: 1C, 2C, 3BWJZ: 1C, 2C, 3BLY: 1C, 2C, 3BFGG: 1A, 1B, 2A, 2C, 3B.

Competing interests

The authors declare no competing interests.

Additional information

Supplementary information The online version contains supplementary material available at https://doi.org/10.1038/s41531-025-01002-2.

Correspondence and requests for materials should be addressed to Guoguang Fan.

Reprints and permissions information is available at http://www.nature.com/reprints

Publisher's note Springer Nature remains neutral with regard to jurisdictional claims in published maps and institutional affiliations.

Open Access This article is licensed under a Creative Commons Attribution-NonCommercial-NoDerivatives 4.0 International License, which permits any non-commercial use, sharing, distribution and reproduction in any medium or format, as long as you give appropriate credit to the original author(s) and the source, provide a link to the Creative Commons licence, and indicate if you modified the licensed material. You do not have permission under this licence to share adapted material derived from this article or parts of it. The images or other third party material in this article are included in the article's Creative Commons licence, unless indicated otherwise in a credit line to the material. If material is not included in the article's Creative Commons licence and your intended use is not permitted by statutory regulation or exceeds the permitted use, you will need to obtain permission directly from the copyright holder. To view a copy of this licence, visit http://creativecommons.org/licenses/by-nc-nd/4.0/.

© The Author(s) 2025